Sensitive detection of magnetic fields including their orientation with a magnetometer based on atomic phase coherence

Hwang Lee,[1,2] Michael Fleischhauer,[1,3] and Marlan O. Scully[1,2]

[1]*Department of Physics, Texas A&M University, College Station, Texas 77843*
[2]*Max-Planck-Institut für Quantenoptik, 85748 Garching, Germany*
[3]*Sektion Physik, Ludwig-Maximilians-Universität, 80333 München, Germany*

An optical magnetometer based on electromagnetically induced transparency is analyzed. Utilizing the different orientation characteristics for different field polarizations, the magnitude *and* orientation of an applied magnetic field can be measured. As a model system we consider the sodium D_1 transition taking into account hyperfine structure and optical pumping effects.
[S1050-2947(98)13209-2]

I. INTRODUCTION

The presence of atomic coherence manifests itself in the optical properties of materials through a plethora of effects such as electromagnetically induced transparency (EIT) [1], enhanced index of refraction [2], lasing without population inversion [3,4], or resonantly enhanced nonlinear processes [5]. Among the interesting applications of these effects is a proposal for a new kind of magnetometer [6,7]. Contrary to the common and established techniques of optical magnetometry [8], it operates in the high-density – strong-field regime leading to potentially higher signal-to-noise ratios. This new type of magnetometer utilizes the high dispersion at an EIT resonance where the absorption is almost completely canceled by quantum interference.

For example, for a simple three-level system, as shown in Fig. 1, the real part of the susceptibility of the probe transition, χ', close to the resonance point, is linear in the two-photon detuning Δ,

$$\chi' \approx -\frac{\wp^2 N}{\hbar \epsilon_0} \frac{\Delta}{\Omega^2}. \tag{1}$$

Here $\wp$ is the dipole matrix element, Ω is the Rabi frequency of the driving field, and N the atomic density. At the same time, as shown in Fig. 1(b), the imaginary part of the susceptibility—which determines the absorption—has a minimum value given by

$$\chi'' \approx \frac{\wp^2 N}{\hbar \epsilon_0} \frac{\gamma_c}{2\Omega^2}. \tag{2}$$

γ_c is the relaxation rate of the lower levels, which can be much smaller than the optical decay rates and thus $\chi'' \to 0$. Since the index of refraction $n = 1 + \chi'/2$ is linear in the two-photon detuning, a relative Zeeman shift of the levels $|c\rangle$ and $|b\rangle$ caused by a magnetic field B leads to a phase shift of the probe field proportional to B,

$$\Delta\phi = \frac{2\pi(n-1)l}{\lambda} = -N\lambda^2 l \frac{3}{4\pi} \frac{\gamma}{\Omega} aB. \tag{3}$$

Here λ is the wavelength of the atomic transition, l the propagation distance, and we have used the relation $\gamma = \wp^2\omega^3/6\pi\hbar\epsilon_0 c^3$ for the radiative decay rate of the upper level. a is a constant containing Bohr's magneton and the Landé factors of the lower levels. Due to the absorption cancellation, high atomic densities can be used, which leads to a large phase shift in the presence of a magnetic field.

For many applications the simultaneous detection of both the direction and the magnitude of small magnetic field fluc-
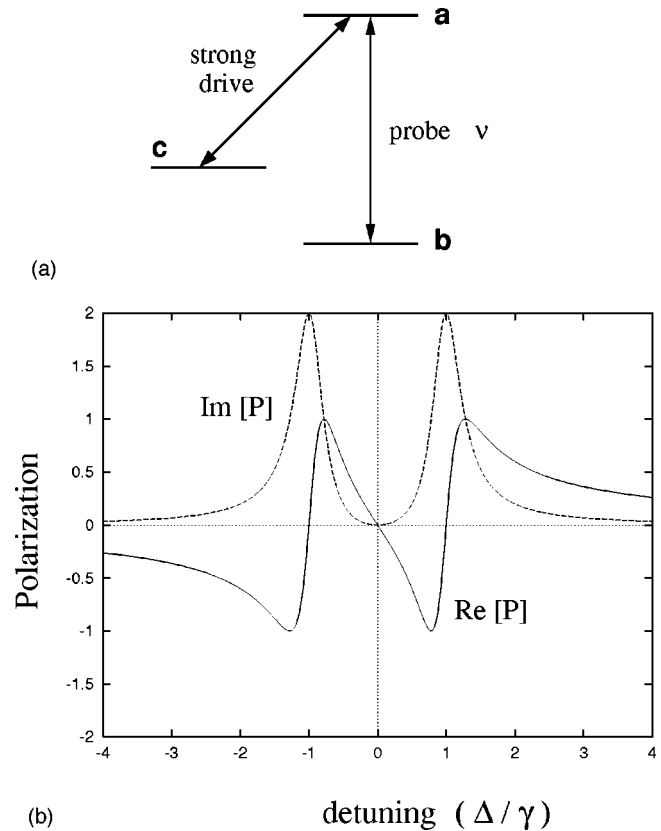

FIG. 1. (a) Level scheme of an EIT resonance. (b) Polarization spectrum (in arbitrary units) of the EIT resonances as a function of atom-field detuning $\Delta = \omega_{ab} - \nu$ for resonant drive field. Im[P] corresponds to absorption, Re[P] to dispersion.
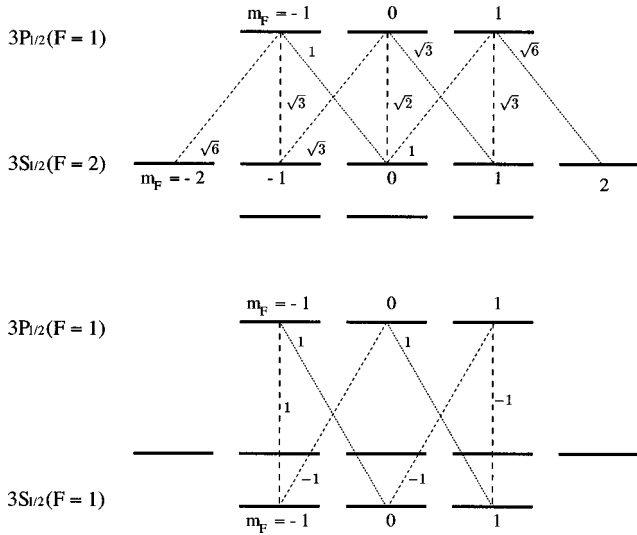
FIG. 2. Relative coupling constants $\wp_{ab} = y\wp$ in sodium hyperfine manifold from the excited state $(3P_{1/2}, F=1)$ to the ground state $(3S_{1/2}, F=1,2)$, where $\wp = 2.3 \times 10^{-30}$ C m; each y value is shown (same as for $\wp_{ac}$).

tuations will be of particular interest [9]. In the present paper, we investigate, therefore, the orientation dependence of the dispersion at an EIT resonance and suggest a particular way to measure the magnetic field *vector*. This is made possible by utilizing the dependence of the atom-field coupling strength of polarized light on the angle between its k vector and the quantization axis of the atoms (direction of the B field). Using a strong driving field, atomic coherence is created within the hyperfine structure of the sodium ground state as in Fig. 2, where the effects of optical pumping and coherent population trapping [10] have to be taken into account. The measured phase shift of a weak probe field in such a configuration will in general depend on the orientation of the magnetic field with respect to the field propagation and the polarizations of the probe and drive fields.

The outline of the paper is as follows. In Sec. II, the probe response of the sodium system including the hyperfine splitting is calculated. Since optical pumping due to the probe field can significantly affect the optical response in a multilevel system, the probe field is taken into account to all orders. In Sec. III, numerical results for the phase shifts of the probe light are presented and the sensitivity of the magnetometer is estimated. In Sec. IV, we discuss a possible method to detect both the magnitude and the direction of the applied magnetic field simultaneously. This method relies on the simultaneous measurement of phase shifts for the left and right circularly polarized components of the probe laser, which have a different orientational characteristics. Finally Sec. V summarizes the results.

II. DISPERSION NEAR AN EIT RESONANCE IN THE SODIUM D_1 MANIFOLD

Both the ground state $(3S_{1/2})$ and the first excited state $(3P_{1/2})$ of sodium have two sublevels $F=1$, $F=2$ as a result of the coupling between the electronic angular momentum $(J=1/2)$ and the nuclear spin $(I=3/2)$. In the present scheme, the $F=1$ levels of the excited state are coupled to

the doublet of the ground state via two resonant radiation fields. The level scheme and the relative transition rates are shown in Fig. 2.

If we apply a magnetic field B whose direction defines the quantization axis, the frequency shift for each hyperfine sublevel is given by

$$\Delta = \frac{\mu_B}{\hbar} m_F g_F B, \qquad (4)$$

where μ_B is the Bohr magneton, m_F is the magnetic quantum number, and g_F is the magnetic g factor given by

$$g_F = g_J \frac{F(F+1) + J(J+1) - I(I+1)}{2F(F+1)},$$

$$g_J = 1 + \frac{J(J+1) + S(S+1) - L(L+1)}{2J(J+1)}. \qquad (5)$$

For our purpose, it is convenient to use shorthand notations for the quantum numbers of the atomic system of sodium, namely

$$|3\,{}^2P_{1/2}, F=1, m_F\rangle = |a, m_a\rangle,$$

$$|3\,{}^2S_{1/2}, F=1, m_F\rangle = |b, m_b\rangle, \qquad (6)$$

$$|3\,{}^2S_{1/2}, F=2, m_F\rangle = |c, m_c\rangle,$$

where $m_a, m_b \in \{-1,0,1\}$ and $m_c \in \{-2,-1,0,1,2\}$.

In the following, a probe laser of frequency ν couples the $F=1$ levels $|a\rangle$ and $|b\rangle$, whereas the $F=2$ levels are coupled to $|a\rangle$ by a strong coherent driving field of frequency ν' propagating in the same direction as the probe field. If the two light beams are left circularly polarized, we have two Λ schemes such as in Fig. 1(a), involving $|a, -1\rangle, |b,0\rangle, |c,0\rangle$, and $|a,0\rangle, |b,1\rangle, |c,1\rangle$. Since for $|b,1\rangle$ and $|c,1\rangle$, g_F has opposite signs and $m_F \neq 0$, the latter configuration will contribute to the two-photon detuning (between $|b\rangle$ and $|c\rangle$) and thus to a phase shift in the presence of a magnetic field .

The atom-field interaction, in the rotating wave approximation, is described by the Hamiltonian

$$\mathcal{H} = \mathcal{H}_0 + \hbar \sum \Omega_{ab} e^{-i\nu t} |a\rangle\langle b|$$

$$+ \hbar \sum \Omega_{ac} e^{-i\nu' t} |a\rangle\langle c| + \text{H.c.}, \qquad (7)$$

with a free term $\mathcal{H}_0$ that includes the magnetic sublevel shifts. In the above short-hand notation, $|a\rangle$ represents all upper levels with different magnetic quantum numbers, and $|b\rangle$ and $|c\rangle$ stand for all lower levels $F=1$ and $F=2$, respectively, as indicated in Eq. (6). The summation runs over all values of m_a, m_b, and m_c, for which the levels are actually coupled by the probe and the drive field. The Rabi frequencies of these transitions are given by

$$\Omega_{ab} = \frac{\wp_{ab}}{\hbar}\mathcal{E}, \quad \Omega_{ac} = \frac{\wp_{ac}}{\hbar}\mathcal{E}_d, \qquad (8)$$

where $\wp_{ab}$ and $\wp_{ac}$ denote the dipole matrix elements between the particular states of the $\{|a\rangle\}$, $\{|b\rangle\}$, and $\{|c\rangle\}$ manifolds, and $\mathcal{E}$ and $\mathcal{E}_d$ are the amplitudes of the probe and drive fields.

To include incoherent relaxation between the atomic levels, we describe the above system by a master equation

$$\dot{\rho} = -\frac{i}{\hbar}[\mathcal{H},\rho] + \mathcal{L}\rho, \qquad (9)$$

where ρ is the density matrix for the atom,

$$\rho = \sum_{l,m_l,l',m_{l'}} |l,m_l\rangle \rho_{lm_l,l'm_{l'}} \langle l',m_{l'}|, \qquad (10)$$

and the operator $\mathcal{L}$ accounts for all the relaxation processes. For instance, for spontaneous decay from $|a\rangle$ to $|b\rangle$, $\mathcal{L}$ has the explicit form

$$\mathcal{L}_{ab}\rho = -\frac{\gamma_{ab}}{2}(|a\rangle\langle a|\rho + \rho|a\rangle\langle a| - 2|b\rangle\langle a|\rho|a\rangle\langle b|), \qquad (11)$$

where we again suppress the indices for the magnetic sublevels. A similar contribution to $\mathcal{L}$ is given by the decay from $|a\rangle$ to $|c\rangle$, or by the thermal and collisional redistribution between $|b\rangle$ and $|c\rangle$, which is particularly relevant in our system. The dispersive properties of sodium, which are illustrated in Figs. 3 and 4, are calculated by solving Eq. (9) numerically. In steady state, Eq. (9) represents a system of linear equations for the coefficients $\rho_{lm_l,l'm_{l'}}$, which can be solved by a simple matrix inversion algorithm.

For left-circularly polarized (LCP) probe light, the complex polarization of the atomic transition $|3^2P_{1/2},F=1\rangle \leftrightarrow |3^2S_{1/2},F=1\rangle$ is related to the density matrix elements via

$$Pe^{-i\nu t} = -N(\wp_{a-1,b0}^* \rho_{a-1,b0} + \wp_{a0,b1}^* \rho_{a0,b1}), \qquad (12)$$

where N is the atomic density, and a similar relation holds for the polarization on the $|3^2P_{1/2},F=1\rangle \leftrightarrow |3^2S_{1/2},F=2\rangle$ transition, which is induced by a coherent LCP driving field. In Figs. 3(a) and 3(b) we show the steady-state values of P for a resonant drive field and different values of the probe field detuning ($\Delta = \omega_{ab} - \nu$). Δ is given in units of γ, the inverse of the lifetime of the $3P_{1/2}$ level, which is 16.4 ns [11], and P in units of $10^{-3}\,N\wp_{ab}$.

Near resonance, the imaginary part of the polarization drops to zero while the real part is linearly proportional to the detuning Δ. This feature is similar to the absorption-dispersion behavior in the simple three-level Λ system as shown in Fig. 1(b). Note, however, the qualitative and quantitative difference between the curves in Fig. 3 and 1. Whereas in the three-level scheme the absorption curve (Im[P]) has two comparably narrow peaks at the points of maximum absorption, for the multilevel configuration these resonances deform into a winglike structure. A similar observation can be made for the refraction curve (Re[P]). The different shape of the curves for the multilevel and the three-level situation is due to the effects of optical pumping and coherent population trapping in the ground-state doublet.
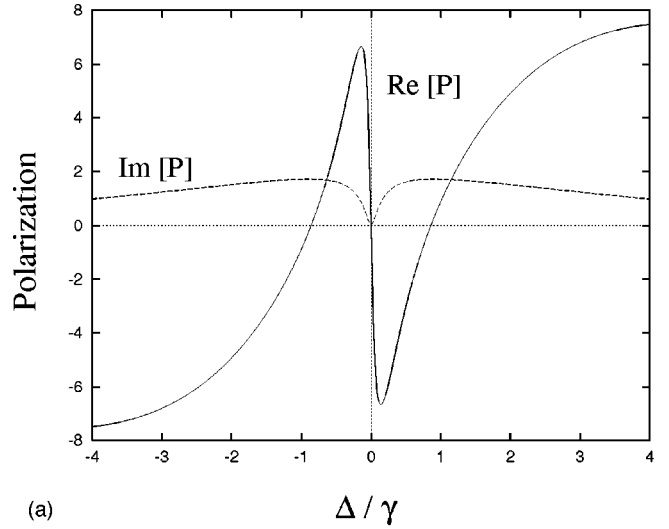

(a)
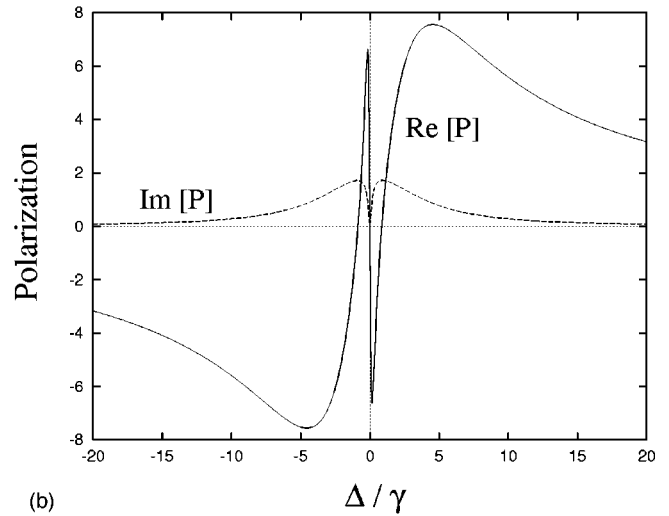
(b)
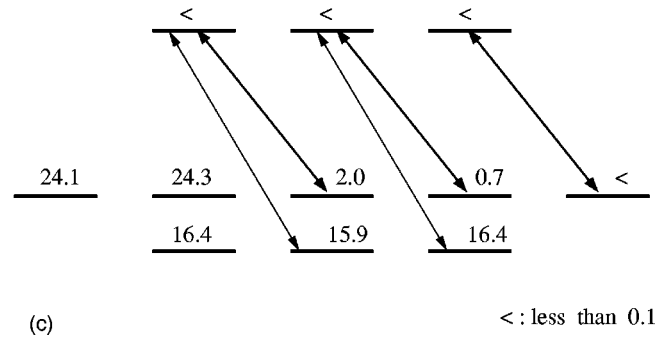
(c)   < : less than 0.1

FIG. 3. (a) Polarization spectrum of sodium D_1 line for resonant drive field as a function of $\Delta = \omega_{ab} - \nu$ in units of $10^{-3}\,N\wp_{ab}$. ($\Omega = 0.2\gamma$, $\Omega_d = \gamma$). (b) Same on a larger scale. (c) Population distribution at resonance $\Delta = 0$.

Figure 3(c) shows the population distribution for exactly resonant probe and drive fields with parameters $\Omega_{ac} = \gamma$, $\Omega_{ab} = 0.2\gamma$, and $\gamma_c = 10^5$ s^{-1} for the collisional (phase) relaxation rate for transitions within the ground-state doublet. Note also that there is significant thermal population of the $|c\rangle = |3^2S_{1/2},F=2\rangle$ multiplet. Due to these effects, the steady-state population strongly depends on the polarization of the applied fields and thus on the direction of the magnetic
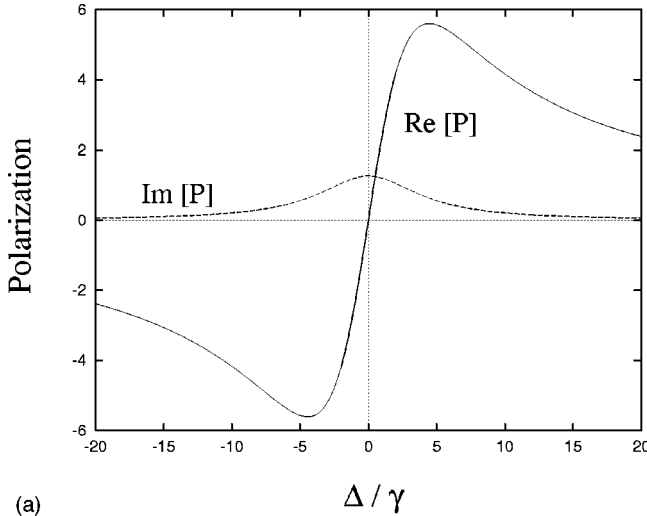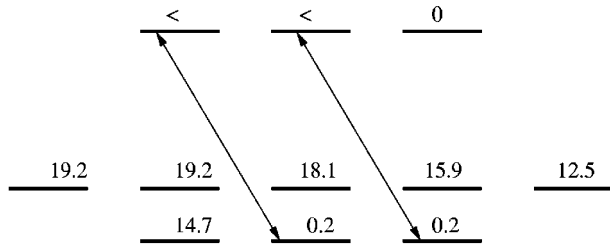
FIG. 4. (a) Polarization spectrum of the sodium D_1 line, with probe field only ($\Omega = 0.2\gamma$), in the same units as in Fig. 3. (b) Corresponding population distribution at resonance $\Delta = 0$.

field with respect to the propagation direction of the lasers. Furthermore, a first order treatment in the probe coupling, which can be applied to the three-level scheme where to zeroth order in the probe field all population is in level b, is generally not valid in the multilevel situation. Here optical pumping caused by the probe field is relevant and needs to be taken into account.

To demonstrate the effect of optical pumping by the probe field we show in Fig. 4(a) the susceptibility curves in the absence of the driving field. In this situation, the population in the $|b,0\rangle$ and $|b,1\rangle$ levels is optically pumped to the other levels of the ground state as can be seen in Fig. 4(b). From Fig. 3(a) we can roughly estimate the dynamical range of the magnetometer. Since the real part of the polarization shows a linear response to the detuning up to $\Delta = 0.14\gamma$, according to Eq. (4) the operation range of the magnetometer will be up to approximately 1 G.

III. ORIENTATION DEPENDENCE AND MAGNETOMETER SENSITIVITY

A probe field propagating along the z axis through a medium of length l will acquire a reduction in amplitude and a phase shift according to

$$\mathcal{E}(z=l) = \kappa \mathcal{E}(z=0)e^{i\Delta\phi}, \tag{13}$$

where κ is the transmittivity of the cell. Within the medium,

the propagation of the field is described by the wave equation, which in the slowly-varying-amplitude approximation reads [12]

$$\left(\frac{\partial}{\partial z} + \frac{1}{c}\frac{\partial}{\partial t}\right)\mathcal{E} = \frac{ik}{2\epsilon_0}P. \tag{14}$$

To calculate the phase shift, we solve Eqs. (9) and (14) self-consistently.

If the propagation direction of the probe field coincides with the direction of the magnetic field to be measured, then, for an LCP probe, the induced polarization involves only two pairs of levels and is related to the atomic density matrix as in Eq. (12). In general, however, there will be a nonzero angle θ between the propagation axis of the laser fields in the medium and the magnetic field. This is particularly important if one wants to follow small fluctuation of a given average magnetic field, and the direction of this fluctuation is not predictable. In this situation, both the probe and driving field will couple to all the magnetic sublevels as is shown in Appendix A. The equations for this situation are, of course, still given by Eqs. (9) and (14), although Eq. (9) now involves all atomic levels and the corresponding relation between the polarization and the density matrix elements is more general than in Eq. (12).

The general solution of these equations is plotted in Fig. 5. There we show the probe phase shift $\Delta\phi$ for two orthogonal polarizations (LCP and RCP) as a function of angle θ and magnitude B of the magnetic field. For the driving field, left-circular polarization (LCP) was chosen. One can see that the dependence of the phase shift on the magnetic field has a different characteristics for an LCP and an RCP probe. We will utilize this fact in the next section to propose a scheme that allows us to simultaneously detect magnitude and direction of B-field fluctuations.

For a fixed angle θ, the phase shift $\Delta\phi$ changes linearly with the strength of the magnetic field, but the slope of this change depends on θ. This linearity reflects the fact that the two-photon detuning induced by the magnetic field stays, for the parameters of Fig. 5, within the linear range near the origin of Fig. 3(a), which defines the operation range of the magnetometer. For a fixed value of B, a cut through Figs. 5(a) and 5(b) parallel to the x-z plane gives the angular dependence of the phase shift. This is shown in detail in Fig. 6, which demonstrates the different directional characteristics of the LCP and the RCP probe.

Before we further discuss these figures in the next section, let us briefly comment on the sensitivity of the magnetometer, which has been discussed in Ref. [7]. As was shown in [7], the minimum detectable phase shift, as determined by shot-noise, is given by

$$\Delta\phi_{min} = \sqrt{\frac{1 + \kappa^2}{2\kappa^2}}\frac{1}{\sqrt{n_{in}}}, \tag{15}$$

where n_{in} is the number of input photons passing through the interferometer per measurement time. This result was obtained by assuming a B field that is parallel to the propagation direction of the laser beams. As can be seen from Fig. 5, the linear response of the signal to a change in B is strongest for $\theta = 0$. For $\theta \neq 0$, this response is generally weaker and
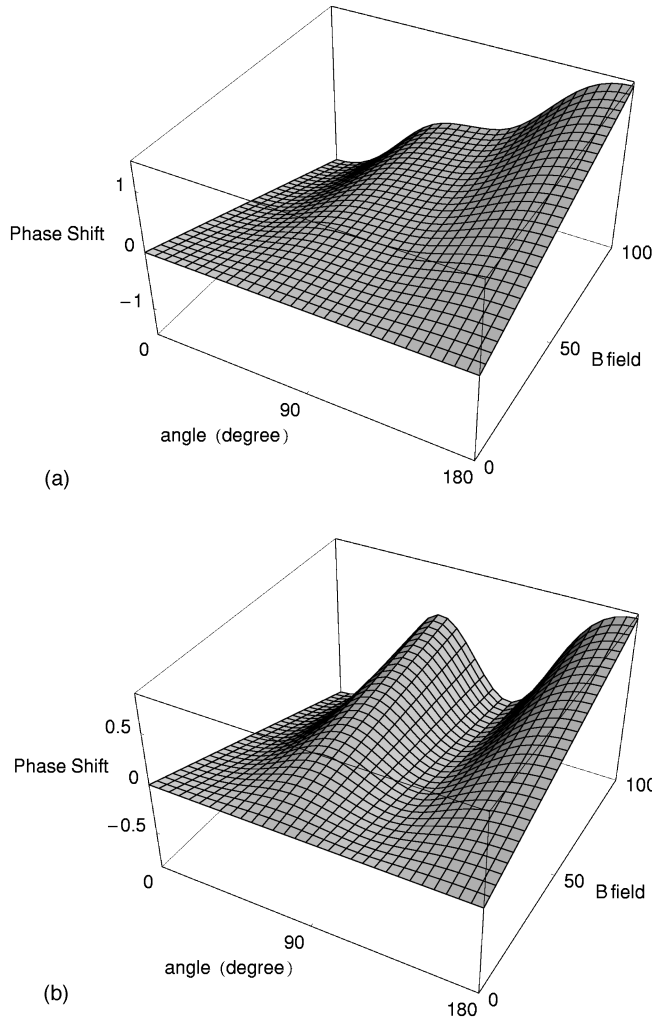
(a)

(b)

FIG. 5. Phase shift of the probe light (in units of 10^{-5}) as a function of magnitude and direction of the B field in the case of an LCP driving field. (a) LCP probe light, (b) RCP probe light (B field in units of 10^{-8} G). Atomic density and length of the medium are chosen to be $N=5\times10^{12}/cm^3$ and $l=10$ cm, respectively. Here and in all the following figures, we have $\kappa \approx 0.9$.

depends on θ. For the singular value $\theta=\pi/2$, when the B field and the laser fields are perpendicular, the probe laser acquires no phase shift at all. The magnetometer will therefore be differently sensitive to changes of the magnetic fields of different direction. For the optimum case $\theta=0$, the ultimate sensitivity of this magnetometer is in the shot-noise limit found to be of the order of 10^{-11} G in a measurement time of 1 s. (An analytic estimate of the sensitivity to first order in the probe field is given in Appendix B.)

Since we deal with atoms in a cell, it is important to consider also the effect of Doppler broadening. A detailed study [7] shows, however, that Doppler broadening plays a negligible role if the probe and driving field propagate in the same direction, the two-photon Doppler-broadening is small, and the drive field is sufficiently strong. These requirements (for details see [7]) are satisfied in the present configuration and we therefore disregard Doppler broadening.

In the present study we have, for simplicity, assumed that the driving-field intensity is controllable to an arbitrary accuracy. In this case we can neglect the effect of ac Stark
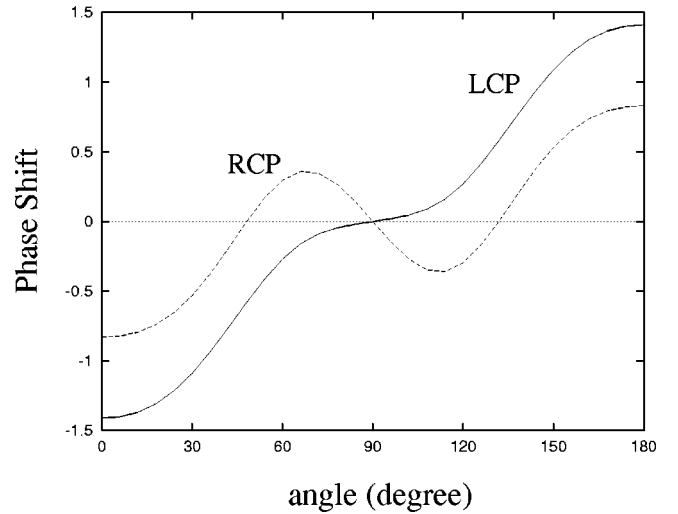

FIG. 6. Phase shifts (in units of 10^{-7}) of RCP and LCP for a given absolute value of the magnetic field (10^{-8} G) as a function of the angle.

shifts from nonresonant couplings. Finite fluctuations of the driving-field intensity, however, give rise to an uncertainty in the susceptibility of the medium. In sodium the most relevant nonresonant couplings are between the hyperfine level $F=2$ of the first excited state $|3P_{1/2}\rangle$ and the ground state. Our numerical studies including these couplings show that for a sensitivity of about 10^{-10} G the intensity of the pump field has to have a short-time stability of 10^{-7}. If we assume a stability of 10^{-4}, the maximum value for the sensitivity reduces to 10^{-7} G. These values can be improved by an order of magnitude if one uses cesium instead of sodium, since the frequency spacing of the nonresonant levels is larger. Note furthermore that the effect of nonresonant ac Stark shifts is much smaller in systems without a hyperfine structure.

Summarizing, we can say that the sensitivity of the magnetometer employing the hyperfine manifold depends crucially on the intensity control of the driving laser. Although the achievable sensitivity in such a configuration is significantly smaller than for atoms without a hyperfine structure [7], it offers a unique way to measure both the magnitude and the direction of a magnetic-field fluctuation simultaneously. This is of interest for various applications and will be discussed in the next section.

IV. SIMULTANEOUS MEASUREMENT OF MAGNITUDE AND DIRECTION

As one can see from Fig. 6, the phase shift corresponding to a magnetic field depends on its direction. If the direction is not known, one cannot uniquely tell what change of the magnetic field was detected for a given phase shift $\Delta\phi$. On the other hand, the different characteristics of the orientation dependence for probe fields with orthogonal polarizations offers a way to measure both the magnitude and the angle (with respect to the propagation axis) of a magnetic field fluctuation simultaneously.

In Figs. 7(a) and 7(b), the contour graphs corresponding to Figs. 5(a) and 5(b) are shown. The contours are obtained by cutting the three-dimensional figure parallel to the x-y
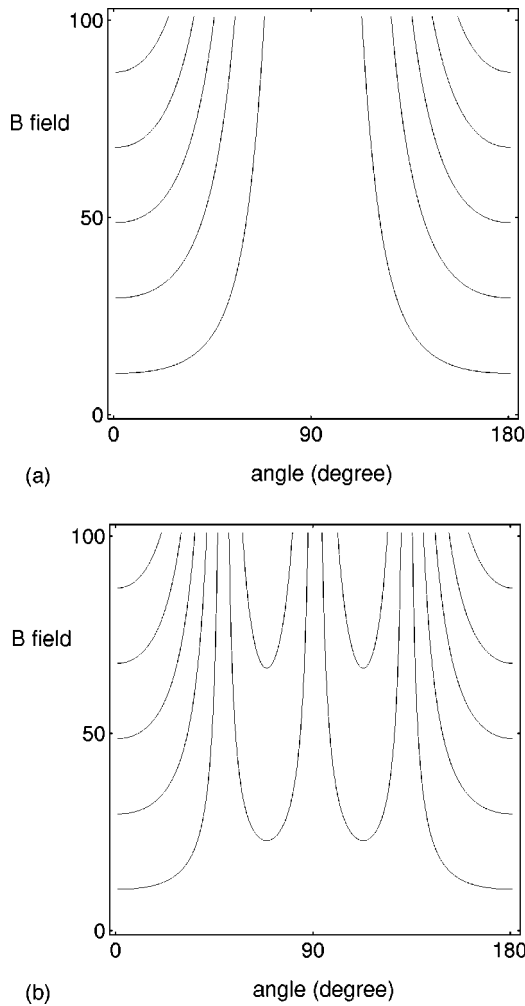
(a)

angle (degree)

(b)

angle (degree)

FIG. 7. Contour graphs corresponding to Fig. 5: (a) RCP, (b) LCP (units are the same as in Fig. 5).
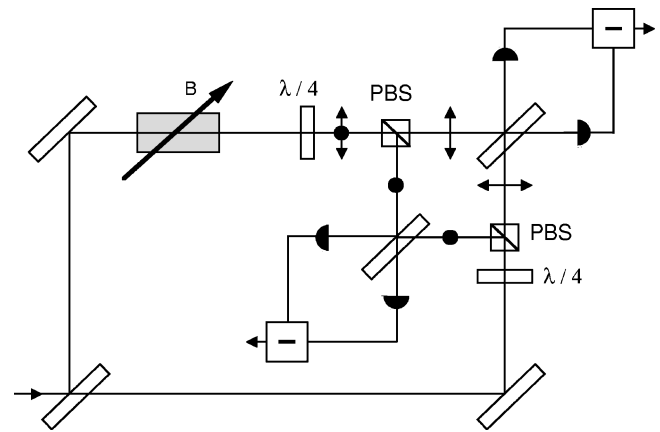

FIG. 8. Schematic setup for simultaneous measurement of the phase shifts for two orthogonal polarizations.

measure the phase shifts one more time after rotating the magnetometer by an arbitrary angle in order to get rid of the axial symmetry.

For some applications it may be inconvenient to first apply an LCP and subsequently an RCP probe laser, and a simultaneous measurement of the corresponding signals is required. If we use, however, an LCP driving field and a *linearly polarized* probe field, which can be regarded as a superposition of right and left circular polarization, it is indeed possible to measure the different phase shifts of each polarization at the same time. In Fig. 8 we provide a possible scheme for a simultaneous measurement of the phase shifts of the two orthogonal polarizations. They are now directed to two different outputs via polarization beam-splitters (PBS), each of them corresponding to one specific circular polarization.

plane, so that each contour corresponds to a specific value of the phase shift. A measured phase shift for LCP light corresponds to one specific contour in magnitude-direction space. Since the measurement of the phase shift for RCP gives another contour in the same space, the crossing point of the two contours yields a unique identification of the detected magnetic field in both magnitude and direction. The only exception is given for changes of the field perpendicular to the laser beam, which lead to no change in $\Delta\phi$ for either the LCP or RCP probe.

We note that our measurement scheme is not restricted to detecting small magnetic fields. Due to the large dynamic range of the magnetometer, it is also possible to observe small variations of a large magnetic fields by tracing the crossing point. Suppose we have a known magnetic field (meaning that we have one point on the contour graph) and there is a small change in the magnetic field. The corresponding signal change of the LCP light leads to a move of the crossing point to another contour line, but we do not yet know the direction of the change in the B field. As soon as we get the signal for RCP (moving to another contour line in the RCP plane), we can find a crossing point again, and we have both the magnitude and the direction of the magnetic field variation with respect to the symmetry axis. If all three spatial components of the B field are required, we need to

V. SUMMARY

In this paper we investigated the orientation dependence of a magnetometer based on atomic phase coherence. As a model case, we analyzed the interaction of two quasiresonant fields with the sodium $|3S_{1/2}\rangle$ and $|3P_{1/2}\rangle$ hyperfine manifolds on the assumption that the fluctuation of the pump field intensity is sufficiently small. The phase shifts for the right and left circularly polarized laser fields have been calculated for an arbitrary orientation of the magnetic field.

Due to the different characteristics of the phase shifts of the two orthogonal circular polarizations, the contour-graph method provides a unique determination of the magnetic field with regard to both its orientation and its amplitude. Hence we can accomplish a simultaneous measurement using two output ports in a Mach-Zehnder interferometer. High sensitivity, a large operation range, and vectorial fluctuation detection make this type of magnetometer a potentially useful tool in many areas of application.

APPENDIX A: ORIENTATION OF THE MAGNETIC FIELD

If the magnetic-field direction has an angle θ with the propagation direction of the light beam (which we chose to be the z axis of our coordinate system), both the driving and the probe field couple to all the magnetic sublevels as shown in Fig. 2. We can simplify the description by introducing an appropriate atomic coordinate system x', y', z' in which the z' axis is parallel to the magnetic field. Taking the x' axis to be the same as the x axis, the unit vectors of these coordinate systems are related by

$$\hat{\mathbf{e}}_x = \hat{\mathbf{e}}'_x,$$

$$\hat{\mathbf{e}}_y = \hat{\mathbf{e}}'_y \cos\,\theta - \hat{\mathbf{e}}'_z \sin\,\theta, \qquad \text{(A1)}$$

$$\hat{\mathbf{e}}_z = \hat{\mathbf{e}}'_y \sin\,\theta + \hat{\mathbf{e}}'_z \cos\,\theta.$$

For the circular polarization, the unit vectors are defined as

$$\hat{\mathbf{e}}_+ = \frac{1}{\sqrt{2}}(\hat{\mathbf{e}}_x - i\hat{\mathbf{e}}_y), \quad \hat{\mathbf{e}}_- = \frac{1}{\sqrt{2}}(\hat{\mathbf{e}}_x + i\hat{\mathbf{e}}_y),$$

$$\text{(A2)}$$

$$\hat{\mathbf{e}}'_+ = \frac{1}{\sqrt{2}}(\hat{\mathbf{e}}'_x - i\hat{\mathbf{e}}'_y), \quad \hat{\mathbf{e}}'_- = \frac{1}{\sqrt{2}}(\hat{\mathbf{e}}'_x + i\hat{\mathbf{e}}'_y),$$

and we have the relations

$$\hat{\mathbf{e}}_\pm = \hat{\mathbf{e}}'_+ \frac{1}{2}(1 \pm \cos\,\theta) \pm \hat{\mathbf{e}}'_z \frac{i}{\sqrt{2}} \sin\,\theta + \hat{\mathbf{e}}'_- \frac{1}{2}(1 \mp \cos\,\theta),$$

$$\text{(A3)}$$

$$\hat{\mathbf{e}}_z = \hat{\mathbf{e}}'_+ \frac{i}{\sqrt{2}} \sin\,\theta + \hat{\mathbf{e}}'_z \cos\,\theta - \hat{\mathbf{e}}'_- \frac{i}{\sqrt{2}} \sin\,\theta.$$

Hence the electric-field components with respect to the atomic z' axis are given by

$$\begin{pmatrix} E'_+ \\ E'_z \\ E'_- \end{pmatrix} = \begin{pmatrix} \frac{1}{2}(1+\cos\,\theta) & \frac{i}{\sqrt{2}}\sin\,\theta & \frac{1}{2}(1-\cos\,\theta) \\ \frac{i}{\sqrt{2}}\sin\,\theta & \cos\,\theta & \frac{-i}{\sqrt{2}}\sin\,\theta \\ \frac{1}{2}(1-\cos\,\theta) & \frac{-i}{\sqrt{2}}\sin\,\theta & \frac{1}{2}(1+\cos\,\theta) \end{pmatrix}$$

$$\times \begin{pmatrix} E_+ \\ E_z \\ E_- \end{pmatrix}, \qquad \text{(A4)}$$

where E_+, E_z, and E_- are the right circularly polarized (RCP), z-polarized, and left circularly polarized (LCP) components of the probe laser, respectively.

APPENDIX B: ANALYSIS TO THE FIRST ORDER IN THE PROBE FIELD

Here we analyze the sodium scheme of Sec. II to first order in the probe field. For simplicity we assume that the collisional decay is only from level $|c\rangle$ to $|b\rangle$. At resonance ($\omega_{a0} - \omega_{b0} = \nu$, $\omega_{a0} - \omega_{c0} = \nu'$), the Hamiltonian in the interaction picture is given by

$$\mathcal{V} = \sum \hbar\Omega_{a,b}e^{i\Delta_{ab}t}|a\rangle\langle b| + \sum \hbar\Omega_{a,c}e^{i\Delta_{ac}t}|a\rangle\langle c| + \text{H.c.,} \tag{B1}$$

where $\Delta_{ab} = \Delta_a - \Delta_b$, $\Delta_a = (\mu_B/\hbar)m_a g_a B$ for each m_a, and so on for subscript b and c. Now using the master equation

$$\dot{\rho} = -\frac{i}{\hbar}[\mathcal{V}, \rho] + \mathcal{L}\rho, \tag{B2}$$

we find ρ_{ab} to the first order in the probe field $\Omega_{a,b}$ in the steady state,

$$\begin{pmatrix} \tilde{\rho}^{(1)}_{a-1,\beta} \\ \tilde{\rho}^{(1)}_{a0,\beta} \\ \tilde{\rho}^{(1)}_{a+1,\beta} \end{pmatrix} = (-i)(M^\beta)^{-1} \begin{pmatrix} \Omega_{a-1,b\beta}/\tilde{\gamma}_{a-1,b\beta} \\ \Omega_{a0,b\beta}/\tilde{\gamma}_{a0,b\beta} \\ \Omega_{a+1,b\beta}/\tilde{\gamma}_{a+1,b\beta} \end{pmatrix} \rho^{(0)}_{b\beta,b\beta} \tag{B3}$$

with $\beta = -1, 0, 1$ from now on. Here we have used the shorthand notations

$$\tilde{\rho}_{a\alpha,b\beta} = \rho_{a\alpha,b\beta}\exp[-i(\Delta_{a\alpha} - \Delta_{b\beta})t],$$

$$\text{(B4)}$$

$$\tilde{\gamma}_{a\alpha,b\beta} = \gamma_{a\alpha,b\beta} + i(\Delta_{a\alpha} - \Delta_{b\beta}),$$

where $\gamma_{a\alpha,b\beta}$ is the off-diagonal decay rate between level $|a,\alpha\rangle$ and $|b,\beta\rangle$, and the subscripts α and β show the magnetic sublevels explicitly. The 3×3 matrix M^β is given as

$$M^\beta_{12} = \frac{1}{\tilde{\gamma}_{a-1,b\beta}}\left[\frac{\Omega_{a-1,c-1}\Omega^*_{a0,c-1}}{\tilde{\gamma}_{c-1,b\beta}} + \frac{\Omega_{a-1,c0}\Omega^*_{a0,c0}}{\tilde{\gamma}_{c0,b\beta}}\right],$$

$$M^\beta_{21} = \frac{1}{\tilde{\gamma}_{a0,b\beta}}\left[\frac{\Omega_{a0,c-1}\Omega^*_{a-1,c-1}}{\tilde{\gamma}_{c-1,b\beta}} + \frac{\Omega_{a0,c0}\Omega^*_{a-1,c0}}{\tilde{\gamma}_{c0,b\beta}}\right],$$

$$M^\beta_{23} = \frac{1}{\tilde{\gamma}_{a0,b\beta}}\left[\frac{\Omega_{a1,c0}\Omega^*_{a0,c0}}{\tilde{\gamma}_{c0,b\beta}} + \frac{\Omega_{a1,c1}\Omega^*_{a0,c1}}{\tilde{\gamma}_{c1,b\beta}}\right], \tag{B5}$$

$$M^\beta_{32} = \frac{1}{\tilde{\gamma}_{a1,b\beta}}\left[\frac{\Omega_{a1,c0}\Omega^*_{a0,c0}}{\tilde{\gamma}_{c0,b\beta}} + \frac{\Omega_{a1,c1}\Omega^*_{a0,c1}}{\tilde{\gamma}_{c1,b\beta}}\right],$$

$$M^\beta_{13} = \frac{1}{\tilde{\gamma}_{a-1,b\beta}}\left[\frac{\Omega_{a-1,c0}\Omega^*_{a1,c0}}{\tilde{\gamma}_{c0,b\beta}}\right],$$

$$M^\beta_{31} = \frac{1}{\tilde{\gamma}_{a1,b\beta}}\left[\frac{\Omega_{a1,c0}\Omega^*_{a-1,c0}}{\tilde{\gamma}_{c0,b\beta}}\right],$$

and

$$M_{\alpha+2,\alpha+2}^{\beta} = \frac{1}{\widetilde{\gamma}_{a\alpha,b\beta}}\left[\frac{|\Omega_{a\alpha,c\alpha-1}|^2}{\widetilde{\gamma}_{c\alpha-1,b\beta}} + \frac{|\Omega_{a\alpha,c\alpha}|^2}{\widetilde{\gamma}_{c\alpha,b\beta}}\right.$$
$$\left. + \frac{|\Omega_{a\alpha,c\alpha+1}|^2}{\widetilde{\gamma}_{c\alpha+1,b\beta}}\right], \tag{B6}$$

where $\alpha = -1,0,1$. The upper level decays radiatively to the lower levels with decay rate γ, and the level $|c\rangle$ decays to the level $|b\rangle$ due to collisions with rate γ_c.

When the magnetic-field direction is parallel to the light-beam direction, with LCP light for both probe and driving field, we obtain from Eq. (B3) that

$$\widetilde{\rho}_{a-1,b0}^{(1)} = \frac{-i\Omega_{a-1,b0}}{\widetilde{\gamma}_{a-1,b0}}\left[\frac{\widetilde{\gamma}_{a-1,b0}\,\widetilde{\gamma}_{c0,b0}}{\widetilde{\gamma}_{a-1,b0}\,\widetilde{\gamma}_{c0,b0} + |\Omega_{a-1,c0}|^2}\right]\rho_{b0,b0}^{(0)}, \tag{B7a}$$

$$\widetilde{\rho}_{a0,b1}^{(1)} = \frac{-i\Omega_{a0,b1}}{\widetilde{\gamma}_{a0,b1}}\left[\frac{\widetilde{\gamma}_{a0,b1}\,\widetilde{\gamma}_{c1,b1}}{\widetilde{\gamma}_{a0,b1}\,\widetilde{\gamma}_{c1,b1} + |\Omega_{a0,c1}|^2}\right]\rho_{b1,b1}^{(0)}. \tag{B7b}$$

For a strong driving field ($|\Omega_{ac}|^2 \gg \gamma\gamma_c$), we can neglect the first term in the denominator. Substituting Eq. (B7) into Eq. (12) (note that here we are in the interaction picture), we obtain from Eq. (13) and Eq. (14) the transmittivity κ and the phase shift $\Delta\phi$ as

$$\kappa = \exp\left\{-\frac{\pi N l}{\lambda\varepsilon_0\hbar}\left[\frac{|\wp_{a0,b1}|^2}{|\Omega_{a0,c1}|^2}\rho_{b1,b1}^{(0)}\gamma_{c1,b1}\right.\right.$$
$$\left.\left. + \frac{|\wp_{a-1,b0}|^2}{|\Omega_{a-1,c0}|^2}\rho_{b0,b0}^{(0)}\gamma_{c0,b0}\right]\right\}, \tag{B8a}$$

$$\Delta\phi = -\frac{\pi N l}{\lambda\varepsilon_0\hbar}\left[\frac{|\wp_{a0,b1}|^2}{|\Omega_{a0,c1}|^2}\rho_{b1,b1}^{(0)}\Delta_{c1,b1}\right.$$
$$\left. + \frac{|\wp_{a-1,b0}|^2}{|\Omega_{a-1,c0}|^2}\rho_{b0,b0}^{(0)}\Delta_{c0,b0}\right], \tag{B8b}$$

where we have used Eq. (8) for the probe field. Taking the coupling constants into account (see Fig. 2) and using $\gamma_{c0,b0} = \gamma_{c1,b1} = \gamma_c/2$ and $\Delta_{c0,b0} = 0$, we find

$$\kappa = \exp\left\{-\frac{2\pi N l\hbar\rho_{b1,b1}^{(0)}}{3\lambda\varepsilon_0|\mathcal{E}_d|^2}\gamma_c\right\}, \tag{B9a}$$

$$\Delta\phi = -\frac{\pi N l\hbar\rho_{b1,b1}^{(0)}}{3\lambda\varepsilon_0|\mathcal{E}_d|^2}\Delta_{c1,b1}, \tag{B9b}$$

where we have assumed equal populations in the $|b\rangle$ levels and again used Eq. (8) as $\mathcal{E}_d$ denotes the driving field amplitude. As one can see in Eq. (B9), the phase shift essentially depends on the absorption

$$\Delta\phi = -\frac{1}{2}\ln\left(\frac{1}{\kappa}\right)\frac{\Delta_{c1,b1}}{\gamma_c}. \tag{B10}$$

From Eqs. (4), (15), and (B10) the minimum detectable magnetic field strength is now given by

$$\frac{\mu_B}{\hbar}(g_c - g_b)B_{\min} = 2\gamma_c\ln^{-1}\left(\frac{1}{\kappa}\right)\sqrt{\frac{1+\kappa^2}{\kappa^2}}\sqrt{\frac{1}{n_{\rm in}}}, \tag{B11}$$

and the minimum is exhibited for $\kappa \approx 0.33$. Under these conditions one can estimate the sensitivity of the magnetometer, which is of order 10^{-11} G, in good agreement with Sec. III.

[1] S. E. Harris, J. E. Field, and A. Imamoğlu, Phys. Rev. Lett. **64**, 1107 (1990); K. J. Boller, A. Imamoğlu, and S. E. Harris, *ibid.* **66**, 2593 (1991); S. E. Harris, J. E. Field, and A. Kasapi, Phys. Rev. A **46**, R29 (1992); for a recent review, see S. E. Harris, Phys. Today **50** (7), 36 (1997).

[2] M. O. Scully, Phys. Rev. Lett. **67**, 1855 (1991); M. O. Scully and S.-Y. Zhu, Opt. Commun. **87**, 134 (1992); M. Fleischhauer, C. H. Keitel, M. O. Scully, C. Su, B. T. Ulrich, and S.-Y. Zhu, Phys. Rev. A **46**, 1468 (1992); A. D. Wilson-Gordon and H. Friedmann, Opt. Commun. **94**, 238 (1992); A. S. Zibrov, M. D. Lukin, L. W. Hollberg, D. E. Nikoniv, M. O. Scully, H. G. Robinson, and V. I. Velichansky, Phys. Rev. Lett. **76**, 3935 (1996).

[3] O. Kocharovskaya and Ya. I. Khanin, Pis'ma Zh. Éksp. Teor. Fiz. **48**, 581 (1988) [JETP Lett. **48**, 630 (1988)]; O. Kocharovskaya and P. Mandel, Phys. Rev. A **42**, 523 (1990); M. Scully, S.-Y. Zhu, and A. Gavrielides, Phys. Rev. Lett. **62**, 2813 (1989); L. M. Narducci, H. M. Doss, P. Ru, M. O. Scully, and C. H. Keitel, Opt. Commun. **81**, 379 (1991); S. E. Harris, Phys. Rev. Lett. **62**, 1033 (1989); A. Imamoğlu and S. Harris, Opt. Lett. **14**, 1344 (1989); A. Lyras, X. Tang, P. Lambropoulos, and J. Zhang, Phys. Rev. A **40**, 4131 (1989); see

also Science **258**, 32 (1992); **263**, 337 (1994); **270**, 737 (1995).

[4] For experimental work, see, for example, A. Nottelmann, C. Peters, and W. Lange, Phys. Rev. Lett. **70**, 1783 (1993); A. S. Zibrov, M. D. Lukin, D. E. Nikonov, L. W. Hollberg, M. O. Scully, and V. L. Velichansky, *ibid.* **75**, 1499 (1995); G. G. Padmabandu, G. R. Welch, I. N. Shubin, E. S. Fry, D. E. Nikonov, M. D. Lukin, and M. O. Scully, *ibid.* **76**, 2053 (1996); P. B. Sellin, G. A. Wilson, K. K. Menduri, and T. W. Mossberg, Phys. Rev. A **54**, 2402 (1996).

[5] S. E. Harris, J. E. Field, and A. Imamoğlu, Phys. Rev. Lett. **64**, 1107 (1990); K. Hakuta, L. Marmet, and B. P. Stoicheff, *ibid.* **66**, 596 (1991); P. Hemmer, D. P. Katz, J. Donoghue, M. Cronin-Golomb, M. Shahriar, and P. Kumar, Opt. Lett. **20**, 982 (1995); M. Jain, M. Xia, G. Y. Yin, A. J. Merriam, and S. E. Harris, Phys. Rev. Lett. **77**, 4326 (1996); M. D. Lukin, M. Fleischhauer, A. S. Zibrov, H. G. Robinson, V. L. Velichansky, L. W. Hollberg, and M. O. Scully, *ibid.* **79**, 2959 (1997).

[6] M. O. Scully and M. Fleischhauer, Phys. Rev. Lett. **69**, 1360 (1992).

[7] M. Fleischhauer and M. O. Scully, Phys. Rev. A **49**, 1973 (1994).

[8] P. A. Franken and F. D. Colegrove, Phys. Rev. Lett. **1**, 316

(1958); F. D. Colegrove and P. A. Franken, Phys. Rev. **119**, 680 (1960); C. Cohen-Tannoudji, J. DuPont-Roc, S. Haroche, and F. Laloë, Phys. Rev. Lett. **15**, 758 (1969); for a review, see E. B. Alexandrov and V. A. Bonch-Bruevich, Opt. Eng. (Bellingham) **31**, 711 (1992).

 [9] See, for example, R. D. Gomez, E. R. Burke, and I. D. Mayergoyz, J. Appl. Phys. **75**, 5910 (1994).

[10] G. Alzetta, A. Gozzini, L. Moi, and G. Orriols, Nuovo Cimento B **36**, 5 (1976); E. Arimondo and G. Orriols, Lett. Nuovo Cimento **7**, 333 (1976); G. Alzetta, L. Moi, and G. Orriols, Nuovo Cimento B **52**, 209 (1979); H. R. Gray, R. M. Whitley, and C. R. Stroud, Jr., Opt. Lett. **3**, 218 (1978); M. P. Radmore and P. L. Knight, J. Phys. B **15**, 561 (1982); Phys. Lett. **102A**, 180 (1984); for a recent review see E. Arimondo, in *Progress in Optics*, edited by E. Wolf (Elsevier Science, Amsterdam, 1996), Vol. XXXV, p. 257.

[11] A. A. Radzig and B. M. Smirnov, *Reference Data on Atoms, Molecules, and Ions* (Springer, Berlin, 1985).

[12] See, for example, M. Sargent III, M. O. Scully, and W. E. Lamb, Jr., *Laser Physics* (Addison-Wesley, Reading, MA, 1974).